

RESEARCH ARTICLE

Temporal contrast enhancement by nonlinear elliptical polarization rotation in a multi-pass cell

Jiajun Song¹, Liya Shen^{1,2}, Jianyu Sun^{1,3}, Yujie Peng¹, and Yuxin Leng¹

¹State Key Laboratory of High Field Laser Physics and CAS Center for Excellence in Ultra-intense Laser Science, Shanghai Institute of Optics and Fine Mechanics (SIOM), Chinese Academy of Sciences (CAS), Shanghai, China

²School of Physical Science and Technology, ShanghaiTech University, Shanghai, China

³Center of Materials Science and Optoelectronics Engineering, University of Chinese Academy of Sciences, Beijing, China

(Received 18 March 2022; revised 25 July 2022; accepted 24 August 2022)

Abstract

We demonstrate the simultaneous temporal contrast improvement and pulse compression of a Yb-doped femtosecond laser via nonlinear elliptical polarization rotation in a solid state multi-pass cell. The temporal contrast is improved to 10^9 , while the pulse is shortened from 181 to 36 fs, corresponding to a compression factor of 5. The output beam features excellent beam quality with M^2 values of 1.18×1.16 . The total efficiency of the contrast enhancement system exceeds 50%. This technique will have wide applications in high temporal contrast ultra-intense femtosecond lasers.

Keywords: multi-pass cell; nonlinear elliptical polarization rotation; pulse compression; temporal contrast

1. Introduction

High-peak-power femtosecond lasers based on chirped pulse amplification (CPA) and optical parametric chirped pulse amplification (OPCPA) technology have developed rapidly in the last few decades^[1–5]. Laser systems with the peak power of 10 petawatt (PW, 1 PW = 10^{15} W) have also been reported in recent years^[6], which have become powerful tools for the investigation of laser–matter interactions. During amplification, unwanted amplified spontaneous emission (ASE) and pre-pulses can be generated and amplified, which deteriorate the temporal contrast of the high-peak-power femtosecond pulse. When the intensity of ASE or pre-pulses reaches 10^{13} W/cm², they can ionize the target material and generate pre-plasma before the main pulse reaches the target, which would seriously affect the laser–matter interactions.

To eliminate negative impact of the undesired pre-pulses and ASE, several temporal pulse cleaning technologies have been proposed and demonstrated, such as cross-polarized wave generation (XPW)^[7,8], optical parametric amplification (OPA)^[9,10], self-diffraction (SD)^[11,12], nonlinear elliptical

polarization rotation (NER)^[13–15], plasma mirrors^[16–18], and nonlinear Fourier filtering^[19,20]. Among the temporal contrast improvement technologies mentioned above, XPW based on the BaF₂ crystal is widely implemented in ultra-intense femtosecond laser facilities worldwide^[5,21], as it improves the temporal contrast by several orders of magnitude and shortens the pulse by a factor of approximately 1.73 at the same time. Therefore, XPW is good for obtaining higher peak power after amplification. Nevertheless, the total efficiency of XPW is typically only about 20%, and the focused intensity of the femtosecond pulse on the BaF₂ crystal is at the 10^{12} W/cm² level, which implies that the damage of the BaF₂ crystal is unavoidable after long-term operation. So, it is necessary to shift the position of the BaF₂ crystal periodically. As for NER, it also features temporal cleaning and spectral broadening simultaneously. Moreover, the spectral broadening capability of NER exceeds that of XPW. Based on NER, the generation of high temporal contrast pulses with few-cycle pulse duration has been reported. In 2019, Smijesh *et al.*^[22] demonstrated the generation of high temporal contrast sub-4 fs pulses by integrating NER into a spectral broadening device of argon filled hollow-core fiber (HCF). In 2020, Khodakovskiy *et al.*^[23] demonstrated the generation of high temporal contrast 5 fs pulses by NER in an HCF compressor. However, the HCF suffers from low transmittance and more complex alignment require-

Correspondence to: Y. Peng, State Key Laboratory of High Field Laser Physics and CAS Center for Excellence in Ultra-intense Laser Science, Shanghai Institute of Optics and Fine Mechanics (SIOM), Chinese Academy of Sciences (CAS), Shanghai 201800, China. E-mail: yjpeng@siom.ac.cn

ments. Another spectral broadening device, called the multi-pass cell (MPC), has been widely investigated in recent years^[24–33]. It consists of two concave mirrors and nonlinear elements between them. The pulse roundtrips inside MPCs can induce dramatic spectral broadening. Compared with HCF, the MPC features high efficiency, excellent energy and power scalability and a low requirement for pointing stability of the input laser. In 2021, Pajer and Kalashnikov^[34] simulated the simultaneous nonlinear spectral broadening and temporal cleaning of femtosecond pulses by NER in an MPC device. In their simulations, 10^3 temporal contrast enhancement with 50% internal efficiency is realized. Recently, Pfaff *et al.*^[35] demonstrated temporal contrast improvement by NER in a gas filled MPC device, and the temporal contrast is enhanced by more than a factor of 50 with an optical efficiency of 56%.

In this paper, the temporal cleaning and compression are experimentally achieved simultaneously by integrating NER into a solid plate-based MPC device. The pedestal of the input pulse is cleaned effectively with a total efficiency higher than 50%, while the pulse duration is shortened from 181 to 36 fs, corresponding to a compression factor of 5. The beam quality after temporal filter is excellent, with M^2 values reaching 1.18×1.16 .

2. Experimental setup

The layout of the experimental setup is depicted in Figure 1. An ytterbium (Yb)-doped femtosecond amplifier is employed as the driving laser, which delivers 2 mJ pulse energy and 181 fs pulse duration at a 1 kHz repetition rate. The central wavelength and the spectral full width at half maximum (FWHM) of the driving laser are 1036.8 and 9.3 nm, respectively. A small portion of pulse energy is used for our proof of principle experiment. The mode matching between the Yb-doped driving laser and eigenmode of the MPC is realized by utilizing three lenses (L1–L3). A Glan prism (GL1) is used to improve the linear polarization degree. The pulse energy after GL1 is 29 μ J. Then, the polarization of the input laser is converted to elliptical through a quarter wave plate (QWP1). The MPC cavity consists of two concave mirrors with 50.8 mm diameter and 300 mm radius of curvature. The MPC mirrors are low group delay dispersion (GDD) coated in the spectral range of 950–1110 nm. The distance between the MPC mirrors is 525 mm, so the eigenmode diameter of the MPC is $2w_1 = 1.023$ mm on the MPC mirrors and $2w_0 = 0.36$ mm in the middle of the MPC. A 5 mm thick fused silica plate coated with high transmittance at 1 μ m is used as the Kerr medium. As material dispersion of the fused silica plate is not compensated inside the MPC, the pulse duration broadens after multiple round trips. The single-pass nonlinear phase shift will decrease gradually. Therefore, a small number of round trips (13) are proposed, corresponding to laser

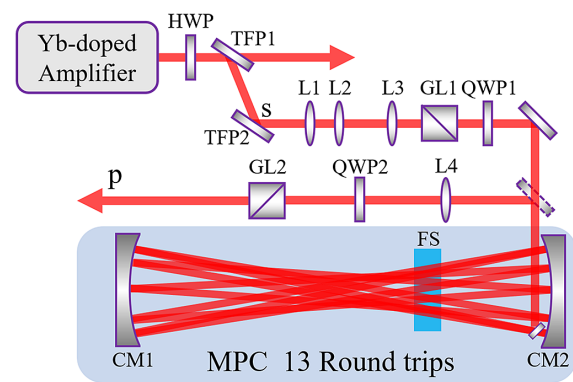


Figure 1. Layout of the experimental setup. HWP, half wave plate; TFP1 and TFP2, thin film polarizers; L1–L4, lenses; GL1 and GL2, Glan prisms; QWP1 and QWP2, quarter wave plates; CM1 and CM2, concave mirrors; FS, fused silica plate.

pulse propagation of 0.13 m in fused silica and 13.5 m in air. It is obvious that the propagation length is much shorter than the respective dispersion lengths of fused silica $L_{D,FS} = 0.64$ m and air $L_{D,air} = 725$ m. The accumulated total material dispersion inside the MPC is calculated to be 2630 fs², which just broadens the input pulse from 181 to 185 fs. As a result, the nonlinear phase shift is barely affected by material dispersion. The pulse coupling in and out of the MPC is performed with a rectangle mirror with 3 mm width. The output beam is collimated with lens L4. Then output pulses are delivered through QWP2 to eliminate the retardation generated by QWP1. The pulse temporally filtered by NER is discriminated by a high extinction ratio ($>2 \times 10^5$) GL2.

3. Experimental results

The output power measured before GL2 is 27.5 mW, corresponding to a transmission efficiency of 95% in the MPC. QWP1, whose optical axis is rotated by an angle γ with respect to the polarization of the input pulse, is employed to set the original ellipticity, while QWP2 is rotated with an angle of $90^\circ + \gamma$. The fused silica plate is positioned at 14, 16, 18 and 20 cm away from CM2, respectively, corresponding to the eigenmode diameter at the position of the plate reducing from 574 to 427 μ m, while ignoring the Kerr lens effect. Therefore, the peak intensity on the plate is estimated to be at the 10^{11} W/cm² level. The total efficiency of the NER filter is investigated as a function of angle γ , and results are described in Figure 2(a). The total efficiency is given by $\eta_t = P_2/P_1$, where P_2 denotes the power after GL2 and P_1 denotes the power after GL1. As the angle γ increases from 0° to 44° , the total efficiency first increases and then decreases. When the fused silica plate is 14 and 16 cm away from CM2, the angle γ corresponding to maximum efficiency is 14° . Angle γ for maximum efficiency shifts to 12° for the plate at 18 and 20 cm away from CM2.

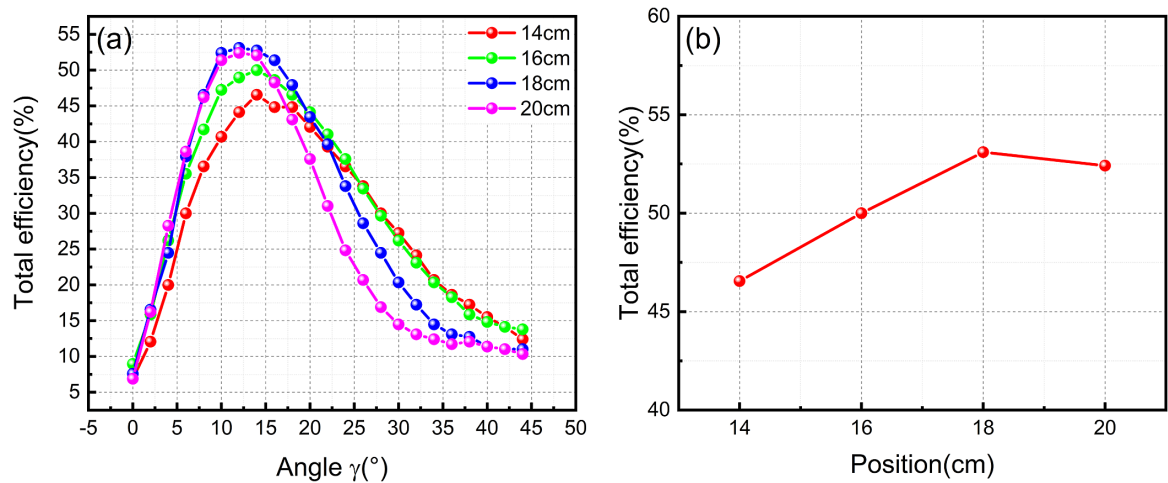


Figure 2. (a) Total efficiency of the NER in the MPC as a function of elliptical angle. (b) Optimum total efficiency when the fused silica plate is placed at different positions.

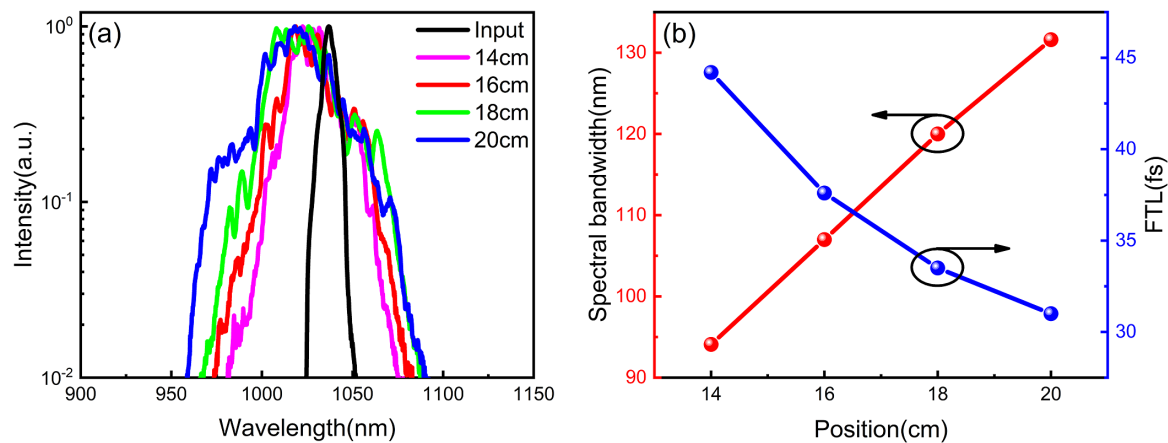


Figure 3. (a) Broadened spectra when the plate is placed at different positions. (b) Spectral bandwidth at the intensity of -20 dB (red line) and the corresponding FTL (blue line).

Figure 2(b) summarizes the optimal total efficiency when the plate is placed at different positions. The highest total efficiency of 53% is obtained when the plate is placed 18 cm away from CM2.

By placing the plate at different positions, the spectra after GL2 are measured at the maximum total efficiency, as presented in Figure 3(a). As the plate moves away from CM2, stronger spectral broadening occurs because the nonlinear phase shift increases gradually. The spectral bandwidth at the intensity of -20 dB is broadened from 94.1 to 131.6 nm, as summarized in Figure 3(b) (red line), and the corresponding Fourier transform limit (FTL) pulse duration is shortened from 44.2 to 31 fs, as shown in Figure 3(b) (blue line). At the strongest spectral broadening condition, the total efficiency of the system is 52%.

After being ejected from the MPC, the positive chirp of the pulse accumulated with propagation through the MPC is compensated by utilizing chirped mirrors. The

pulse duration is characterized by using a homebuilt second harmonic frequency-resolved optical gating (SHG-FROG) device. A pulse duration of 36 fs is obtained when the compensated GDD is -3200 fs², corresponding to a compression factor of 5. The measured and retrieved traces are shown in Figures 4(a) and 4(b). The spectral intensity and phase are shown in Figure 4(c). The input pulse, compressed pulse and calculated FTL pulse durations are presented in Figure 4(d).

The beam quality (M^2) of the temporally cleaned pulse is measured to be 1.18×1.16 by employing a commercial M -squared factor meter (BSQ-SP300, Ophir Spiricon), which is shown in Figure 5. Compared with the M^2 of the input laser, the beam quality is almost maintained.

The energy of the temporally cleaned pulse is no more than 20 μ J, which is insufficient to perform temporal contrast measurement with a commercial third-order cross-correlator device. So, a Yb:KGW-based chirped pulse amplifier was

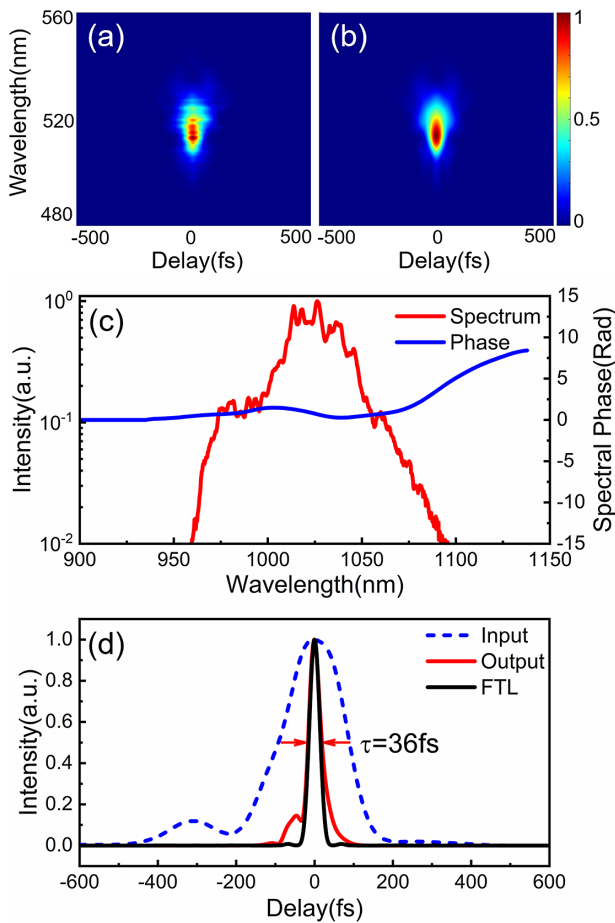


Figure 4. SHG-FROG characterization of the filtered pulse. (a) Measured and (b) retrieved SHG-FROG traces (0.45% FROG error on a 512×512 grid). (c) Measured spectrum (red line) and spectral phase (blue line). (d) Input pulse duration (blue dashed line), retrieved pulse duration (red line) and calculated FTL pulse duration (black line).

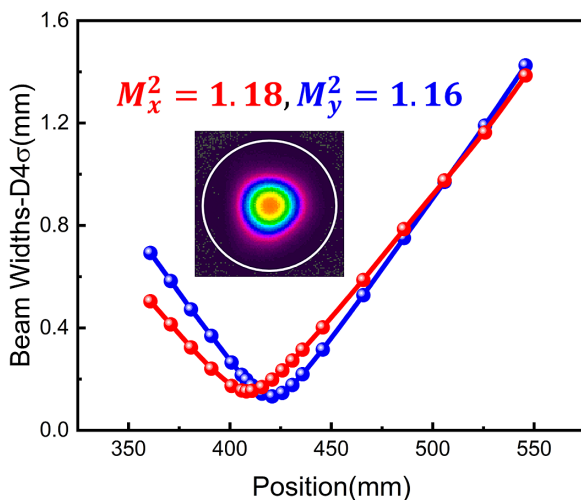


Figure 5. Beam quality after the MPC device.

built to boost the filtered pulse energy. The schematic of the amplifier is depicted in Figure 6. The stretcher and compressor share one transmission grating. One Ng-cut

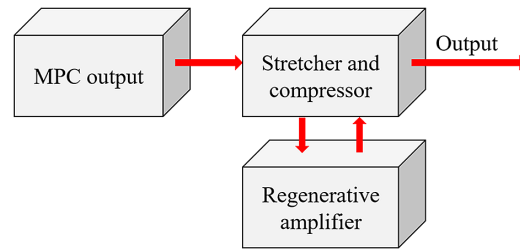


Figure 6. Schematic of the Yb:KGW chirped pulse amplifier.

Yb:KGW crystal with a size of $3 \text{ mm} \times 3 \text{ mm} \times 5 \text{ mm}$ is employed as a gain medium in the regenerative amplifier. The dumped pulse energy of the regenerative cavity is $800 \mu\text{J}$. Limited by the emission spectral bandwidth of the Yb:KGW crystal and gain narrowing, the spectral bandwidth of the amplified pulse is narrowed to 4.8 nm , as shown in Figure 7(a). Assuming a sech^2 shaped pulse, the compressed pulse duration is 457 fs , as shown in Figure 7(b).

Figure 8 shows the measured temporal contrast of the amplified pulse (red line), which is 10^9 . As a comparison, the temporal contrast is 10^7 when the amplifier is seeded by a semiconductor saturable absorption mirror (SESAM) mode-locked fiber oscillator (black line). It can be seen that the fluctuation of the ASE intensity increases dramatically when employing the temporally cleaned pulse as the seed. This is because the distance between the Yb-doped driving laser and the homemade Yb:KGW regenerative amplifier is around 10 m , which deteriorates the energy stability of the amplified pulse.

4. Conclusion

In conclusion, the temporal contrast of a Yb-doped femtosecond laser is enhanced to nearly 10^9 by integrating NER into a solid-state MPC device. The pulse duration is compressed from 181 to 36 fs , corresponding to a compression factor of 5 . The beam quality after the MPC is excellent, with the M^2 value of 1.18×1.16 . The total efficiency of the MPC-based temporal contrast enhancement device is higher than 50% . Benefitting from excellent power and energy scalability of the MPC device, we believe that this scheme can be applied to high-energy pulse cleaning system.

Acknowledgments

This work was supported by the National Key R&D Program of China (No. 2017YFE0123700), the National Natural Science Foundation of China (Nos. 61925507 and 62075227), the Shanghai Rising-Star Program (No. 21QA1410200), and the Youth Innovation Promotion Association CAS (No. 2020248).

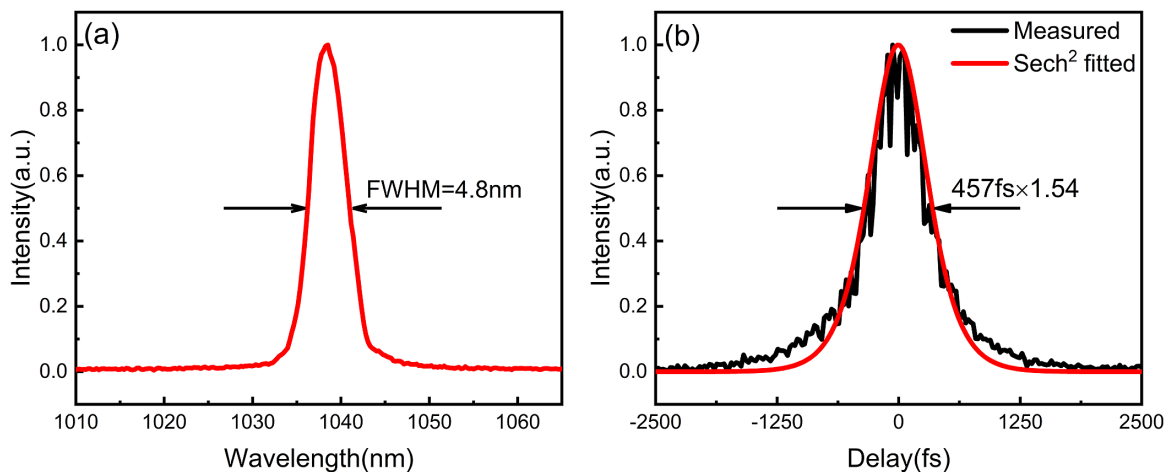


Figure 7. (a) Spectrum and (b) pulse duration of the Yb:KGW amplifier.

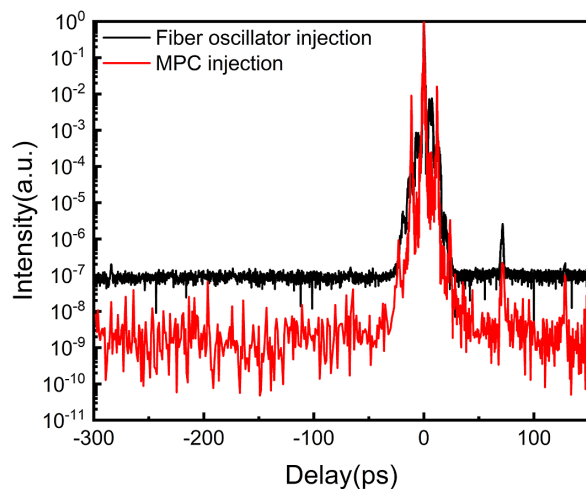


Figure 8. Temporal contrast of the homemade Yb:KGW amplifier with different seed injections.

References

1. Y. Wang, S. Wang, A. Rockwood, B. M. Luther, R. Hollinger, A. Curtis, C. Calvi, C. S. Menoni, and J. J. Rocca, *Opt. Lett.* **42**, 3828 (2017).
2. Z. H. Wang, C. Liu, Z. W. Shen, Q. Zhang, H. Teng, and Z. Y. Wei, *Opt. Lett.* **36**, 3194 (2011).
3. H. Kiriya, A. S. Pirozhkov, M. Nishiuchi, Y. Fukuda, K. Ogura, A. Sagisaka, Y. Miyasaka, M. Mori, H. Sakaki, N. P. Dover, K. Kondo, J. K. Koga, T. Z. Esirkepov, M. Kando, and K. Kondo, *Opt. Lett.* **43**, 2595 (2018).
4. F. Batysta, R. Antipenkov, T. Borger, A. Kissinger, J. T. Green, R. Kananavicius, G. Cheriaux, D. Hiding, J. Kolenda, E. Gaul, B. Rus, and T. Ditmire, *Opt. Lett.* **43**, 3866 (2018).
5. J. H. Sung, H. W. Lee, J. Y. Yoo, J. W. Yoon, C. W. Lee, J. M. Yang, Y. J. Son, Y. H. Jang, S. K. Lee, and C. H. Nam, *Opt. Lett.* **42**, 2058 (2017).
6. W. Q. Li, Z. B. Gan, L. H. Yu, C. Wang, Y. Q. Liu, Z. Guo, L. Xu, M. Xu, Y. Hang, Y. Xu, J. Y. Wang, P. Huang, H. Cao, B. Yao, X. B. Zhang, L. R. Chen, Y. H. Tang, S. Li, X. Y. Liu, S. M. Li, M. Z. He, D. J. Yin, X. Y. Liang, Y. X. Leng, R. X. Li, and Z. Z. Xu, *Opt. Lett.* **43**, 5681 (2018).
7. L. P. Ramirez, D. N. Papadopoulos, A. Pellegrina, P. Georges, F. Druon, P. Monot, A. Ricci, A. Jullien, X. Chen, J. P. Rousseau, and R. Lopez-Martens, *Opt. Express* **19**, 93 (2011).
8. G. I. Petrov, O. Albert, J. Etchepare, and S. M. Saltiel, *Opt. Lett.* **26**, 355 (2001).
9. C. Liu, Z. Wang, W. Li, Q. Zhang, H. Han, H. Teng, and Z. Wei, *Opt. Lett.* **35**, 3096 (2010).
10. J. Hu, X. Wang, X. Yang, P. Bai, F. Wu, Z. Zhang, H. Chen, X. Yang, J. Qian, J. Gui, Y. Li, Y. Liu, X. Lu, Y. Xu, and Y. Leng, *Opt. Express* **29**, 37443 (2021).
11. X. Z. Wang, Z. H. Wang, Y. Y. Wang, X. Zhang, J. J. Song, and Z. Y. Wei, *Chin. Phys. Lett.* **38**, 074202 (2021).
12. J. Liu, K. Okamura, Y. Kida, and T. Kobayashi, *Opt. Express* **18**, 22245 (2010).
13. D. Homoelle, A. L. Gaeta, V. Yanovsky, and G. Mourou, *Opt. Lett.* **27**, 1646 (2002).
14. A. Jullien, F. Auge-Rochereau, G. Cheriaux, J. P. Chambaret, P. d'Oliveira, T. Auguste, and F. Falcoz, *Opt. Lett.* **29**, 2184 (2004).
15. M. P. Kalashnikov, E. Risse, H. Schonngel, and W. Sandner, *Opt. Lett.* **30**, 923 (2005).
16. A. Lévy, T. Ceccotti, P. D'Oliveira, F. Réau, M. Perdrix, F. Quéré, P. Monot, M. Bougeard, H. Lagadec, and P. J. O. L. Martin, *Opt. Lett.* **32**, 310 (2007).
17. B. Dromey, S. Kar, M. Zepf, and P. Foster, *Rev. Sci. Instrum.* **75**, 645 (2004).
18. C. Rödel, M. Heyer, M. Behmke, M. Kübel, O. Jäckel, W. Ziegler, D. Ehrt, M. Kaluza, and G. Paulus, *Appl. Phys. B* **103**, 295 (2011).
19. B. Gilicze, R. Dajka, I. B. Foldes, and S. Szatmari, *Opt. Express* **25**, 20791 (2017).
20. S. Szatmari, R. Dajka, A. Barna, B. Gilicze, and I. B. Foldes, *Laser Phys. Lett.* **13**, 075301 (2016).
21. L. P. Yu, Y. Xu, Y. Q. Liu, Y. Y. Li, S. Li, Z. Z. Liu, W. K. Li, F. X. Wu, X. J. Yang, Y. L. Yang, C. Wang, X. M. Lu, Y. X. Leng, R. X. Li, and Z. Z. Xu, *Opt. Express* **26**, 2625 (2018).
22. N. Smijesh, X. Zhang, P. Fischer, A. A. Muschet, R. Salh, A. Tajalli, U. Morgner, and L. Veisz, *Opt. Lett.* **44**, 4028 (2019).
23. N. G. Khodakovskiy, M. P. Kalashnikov, V. Pajer, A. Blumenstein, P. Simon, M. M. Toktamis, M. Lozano, B. Mercier, Z. Cheng, T. Nagy, and R. Lopez-Martens, *Laser Phys. Lett.* **16**, 095001 (2019).
24. J. Schulte, T. Sartorius, J. Weitenberg, A. Vernaleken, and P. Russbuedt, *Opt. Lett.* **41**, 4511 (2016).
25. M. Hanna, X. Delen, L. Lavenue, F. Guichard, Y. Zaouter, F. Druon, and P. Georges, *J. Opt. Soc. Am. B* **34**, 1340 (2017).

26. J. Weitenberg, A. Vernaleken, J. Schulte, A. Ozawa, T. Sartorius, V. Pervak, H. D. Hoffmann, T. Udem, P. Russbuldt, and T. W. Hansch, *Opt. Express* **25**, 20502 (2017).
27. C. L. Tsai, F. Meyer, A. Omar, Y. C. Wang, A. Y. Liang, C. H. Lu, M. Hoffmann, S. D. Yang, and C. J. Saraceno, *Opt. Lett.* **44**, 4115 (2019).
28. L. Lavenu, M. Natile, F. Guichard, Y. Zaouter, X. Delen, M. Hanna, E. Mottay, and P. Georges, *Opt. Lett.* **43**, 2252 (2018).
29. P. Balla, A. B. Wahid, I. Sytceвич, C. Guo, A. L. Viotti, L. Silletti, A. Cartella, S. Alisauskas, H. Tavakol, U. Grosse-Wortmann, A. Schonberg, M. Seidel, A. Trabattoni, B. Manschwetus, T. Lang, F. Calegari, A. Couairon, A. L'Huillier, C. L. Arnold, I. Hartl, and C. M. Heyl, *Opt. Lett.* **45**, 2572 (2020).
30. S. Gröbmeyer, K. Fritsch, B. Schneider, M. Poetzlberger, V. Pervak, J. Brons, and O. Pronin, *Appl. Phys. B* **126**, 159 (2020).
31. J. Weitenberg, T. Saule, J. Schulte, and P. Russbuldt, *IEEE J. Quantum Electron.* **53**, 1 (2017).
32. J. Song, Z. Wang, X. Wang, R. Lü, H. Teng, J. Zhu, and Z. Wei, *Chin. Opt. Lett.* **19**, 093201 (2021).
33. J. Song, Z. Wang, R. Lv, X. Wang, H. Teng, J. Zhu, and Z. Wei, *Appl. Phys. B* **127**, 50 (2021).
34. V. Pajer and M. Kalashnikov, *Laser Phys. Lett.* **18**, 065401 (2021).
35. Y. Pfaff, C. Forster, G. Barbiero, M. Rampp, S. Klingebiel, J. Brons, C. Y. Teisset, H. C. Wang, R. Jung, J. Jaksic, A. H. Woldegeorgis, C. J. Saraceno, and T. Metzger, *Opt. Express* **30**, 10981 (2022).